POLITECNICO DI TORINO
Repository ISTITUZIONALE

Turbulence-distortion analysis for leading-edge noise-prediction enhancement

(Article begins on next page)

17 October 2023

Turbulence-distortion analysis for leading-edge noise-prediction enhancement

Andrea Piccolo[*]
Delft University of Technology, Delft, 2629HS, Netherlands

Riccardo Zamponi[†]
Delft University of Technology, Delft, 2629HS, Netherlands
von Karman Institute for Fluid Dynamics, Sint-Genesius-Rode, B-1640, Belgium

Francesco Avallone[‡]
Politecnico di Torino, Torino, 10129, Italy

Daniele Ragni[§]
Delft University of Technology, Delft, 2629HS, Netherlands

The analytical model for leading-edge noise prediction formulated by Amiet, developed for a flat plate, relates the far-field acoustic pressure to the upstream inflow conditions, modeled by canonical turbulence spectra. The inaccurate results provided by this low-fidelity method when applied to thick airfoils has been attributed to the distortion experienced by turbulent structures when approaching the airfoil, not modeled in the original formulation of Amiet. The first attempts to account for the effects of this physical mechanism consisted of modifying the term representing the incoming turbulence by means of the analytical results of the rapid distortion theory, obtaining a promising improvement of the noise-prediction accuracy.

This paper aims to set up the physical framework to investigate the relation between turbulence distortion and noise-generation mechanisms with the purpose of enhancing inflow-turbulence noise modeling. A numerical database obtained for a rod-airfoil configuration has been chosen to allow the analysis of the vortex dynamics when interacting with a body. The analysis of the velocity field near the leading edge has highlighted that the extension of the region where turbulence distortion occurs depends on the size of the incoming turbulence structures. Furthermore, surface pressure fluctuations have been observed to peak at the same position along the airfoil where the pressure gradient in the streamwise direction is maximum. A novel approach has been proposed to account for turbulence distortion in Amiet's model by using as input the turbulence spectrum directly sampled in this position. A satisfactory agreement with the prediction provided by the solid formulation of the Ffowcs-Williams and Hawkings analogy has been obtained.

I. Introduction

Tʜᴇ noise generated by wind turbines represents one of the most significant obstacles to the diffusion of onshore wind energy as a well-established alternative energy source. Wind turbines acoustic performances are mostly affected by aeroacoustic sources, with respect to mechanical ones [1–3], with several and physically different unsteady flow mechanisms contributing to the noise generation.

The present work focuses on turbulent inflow noise, also defined as leading-edge noise, related to the interaction of the blade with turbulence in the incoming flow. In the case of wind turbines, turbulence may be due to the atmospheric boundary layer, the wake of upwind turbines in a wind farm, or the wakes from trees and buildings in case of installations close to urban environments [4–6]. The accurate physical modeling of this flow-induced noise source could bring a significant improvement to the state-of-the-art of noise-prediction methods, and this is the reason why it is still the

---

*PhD Candidate, Flow Physics and Technology Department, a.piccolo@tudelft.nl.

†Assistant Professor, Flow Physics and Technology Department, r.zamponi@tudelft.nl, AIAA Member.

‡Assistant Professor, Department of Mechanical and Aerospace Engineering, francesco.avallone@polito.it, AIAA Member.

§Associate Professor, Flow Physics and Technology Department, d.ragni@tudelft.nl, AIAA Member.

subject of significant research [2, 7–12]. Indeed, industrial applications mainly account for this noise mechanism by means of analytical models, which relate the far-field noise to a statistical description of the incoming velocity field [7, 13–15], hence neglecting possible effects of the body geometry on the flow behaviour. This is the case of the analytical model developed by Amiet [7], which is at the base of many currently implemented low-fidelity approaches. The method is based on the response to incoming perturbations of a flat plate, and it has been shown to be less accurate in the case of thick airfoils [15–17].

Paterson and Amiet [14] showed that, for a NACA-0012 airfoil, Amiet's model provides accurate predictions for high Mach numbers. However, noise is overestimated at higher frequencies as the flow velocity decreases. An order-of-magnitude criterion for the breakdown of the theory was identified where the size of the eddies becomes comparable with the airfoil thickness, i.e., when $U/ft \leq 1$, U being the mean flow velocity, f the sound frequency and t the airfoil thickness. The discrepancy between experimental measurements and low-fidelity prediction has also been observed in the low-frequency range for a full-scale wind turbine. Buck *et al.* [18] tested a 2.3 MW wind turbine and compared the measurements with the results provided by Amiet's theory. Interestingly, the study showed that inflow-turbulence noise is dominant in the low-frequency range (up to 450 Hz for the considered application), where the model, despite a correct estimation of the slope of the spectra, yielded a general underestimation of 5 dB with respect to the experimental spectra.

The distortion of the turbulent structures caused by the presence of the airfoil has been assumed to affect leading-edge noise generation [10, 11, 19]. The reduced accuracy of the prediction provided by low-fidelity methods for thick airfoils could be hence explained by the fact that the previous mechanism is not properly taken into account in the noise generation modeling. A thorough understanding of the effects of turbulence distortion could hence identify a possible enhancement for leading-edge noise prediction models. In this regard, an effective analytical framework that can be employed to calculate the turbulence distortion around an airfoil with a nonnegligible thickness is the rapid distortion theory (RDT), originally formulated by Hunt [20]. In his work, Hunt carried out a wavenumber analysis to compute the homogeneous turbulent flow past a cylinder. Velocity spectra and variances were derived in the asymptotic cases where the turbulence integral length scale L can be considered much smaller or larger than the characteristic dimension of the bluff body a. From a physical point of view, the results of this investigation (validated by several experimental studies [21, 22]) identified different mechanisms with which the turbulent structures are deformed according to the above-mentioned ratio L/a. In particular, for $L/a \gg 1$, the prevailing distortion mechanism is due to the blockage imposed by the presence of the body. This mechanism causes a momentum transfer between the streamwise and the upwash velocity components of a fluid element approaching the airfoil along the stagnation streamline. As a result, the streamwise-velocity fluctuations decrease near the surface, while the upwash ones increase. For small-scale structures ($L/a \ll 1$), the dominant distortion mechanism is instead determined by the deformation of the vorticity field due to the deflection of the streamlines upstream and around the body. The altered vorticity field, in turn, induces changes in the velocity fluctuations depending on the stretching or shortening of the vortex lines as they are convected towards the body. In particular, the streamwise- and spanwise-velocity fluctuations increase, while the upwash ones decrease.

The first attempts to use the findings of the RDT to enhance leading-edge noise prediction consisted of modifying the spectrum used to describe the upstream flow conditions in Amiet's model. More specifically, the analytical expression of the canonical turbulence spectrum was modified using the results of the RDT and scaled with statistical quantities sampled nearby the airfoil. This approach was proposed by Moreau and Roger [10], who formulated a correction to the von Karman spectrum with the purpose of including the effects caused by turbulence distortion in the case of a NACA-0012. A good agreement with the experimental measurements was achieved by applying Amiet's model with this modified spectrum as input. A similar procedure was also followed by Christophe [19] and de Santana *et al.* [11], who used the findings of Hunt for the small-scale structures asymptotic case to modify the von Karman spectrum, which was then scaled sampling the turbulence intensity and integral length scale in the vicinity of the airfoil leading edge. Amiet's model using this spectrum in input yielded a better match with the experimental results with respect to the original formulation.

Despite these promising results, these works were mainly focused on the modification of Amiet's model and the alteration of the velocity field, and no extended physical analysis was performed to assess the impact of turbulence distortion on the noise generation mechanisms and hence generalize the result.

The goals of the present work are to understand the behavior of turbulence in the interaction with the leading edge of the airfoil to assess the effects of distortion on the noise generation and to determine the potential benefits, in terms of accuracy, of including this physical mechanism into the leading-edge noise prediction. This analysis has been hence completed by applying Amiet's model considering in input a turbulence frequency spectrum sampled in the region where turbulence distortion is occurring.

To pursue these objectives, an existing numerical lattice-Boltzmann Method (LBM) database developed and validated by Teruna *et al.* [23] has been considered. The dataset consists of a rod-airfoil configuration reproducing the benchmark arrangement proposed by Jacob *et al.* [24] where a NACA-0012 airfoil interacts with the turbulence shed by an upstream cylinder. The resulting sound field is thus characterized by broadband noise dominated by a shedding frequency.

The present paper is structured as follows. First, the developed methodology is explained in detail in Section II. The achieved results are reported and discussed in Section III. Finally, the conclusions are drawn in Section IV.

II. Methodology

A. Flow Solver

The flow field around the airfoil has been computed using the commercial software 3DS Simulia PowerFLOW 5.4b, previously used for analyzing other wake-body interaction cases [25–27]. Lattice-Boltzmann equations, which compute the advection and collision of fluid particles using a statistical gas kinetic model, are at the base of the numerical technique. The discretization has been performed using 19 discrete velocities in three dimensions (D3Q19), using a third-order truncation of the Chapman-Enskog expansion [28]. The explicit time integration and collision model based on Bhatnagar-Gross-Krook (BGK) [29] are used. This model introduces a relaxation of the particle distribution function towards that of Maxwell-Boltzmann that describes gas particles at rest. Flow variables are calculated by integrating the particle distribution functions over the 19 discrete state directions. Turbulent fluctuations are modeled by extending the lattice-Boltzman Method (LBM) to include an effective turbulent relaxation time [30], which replaces that in the BGK model. The effective relaxation time is computed using the two-equation $k - \epsilon$ renormalization group [31] model. The nonlinearity of the Reynolds stresses can be hence taken into account by this procedure, which is subsequently referred to as very-large eddy simulation (VLES) [32].

The lattice-Boltzmann scheme is applied on a unit lattice defined as *voxel*. The dimension of this volumetric element in adjacent resolution regions of the simulation domain varies by a factor of 2. Surface elements referred as *surfels* are used to discretize surfaces of solid bodies in the positions where they are intersected by a voxel. The fluid particle interaction with the solid surface is governed by the wall-boundary condition, such as particle bounce-back process for no-slip wall and specular reflection for slip wall [33]. The wall-shear stress is approximated by means of a wall function applied on the first wall-adjacent grid. The function is based on the generalized law-of-the-wall model [34], extended to consider the effects of pressure gradient and surface roughness.

The Ffowcs-Williams and Hawkings (FW-H) acoustic analogy [35] in the formulation 1A of Farassat and Succi [36] with forward-time solution [37] has been utilized to compute far-field noise. The sound sources have been considered both on a permeable surface enclosing rod and airfoil in the near-field region and on the airfoil surface. In the former application, the contribution of dipole sources at the surface of solid objects and of quadrupole sources in the turbulent-flow field have been considered, whereas, in the latter, only the dipole sources acting on the airfoil surface have been taken into account.

B. Simulation setup and post-processing

As mentioned in Section I, the configuration studied by Teruna *et al.* [23], validated using experimental and numerical works, uses the same rod-airfoil setup considered by Jacob *et al.* [24] to analyze the noise reduction obtained using leading-edge serrations and porous materials.

In the present work, the airfoil is a NACA-0012 with solid leading edge with a chord $c = 0.1$ m, whereas the rod has a diameter $d_{\mathrm{rod}} = 0.01$ m. The radius of the leading edge is calculated considering the thickness and chord of the airfoil as $r_{\mathrm{LE}} = 1.1019\, t_{\mathrm{airfoil}}^2 c$, which yields $r_{\mathrm{LE}} = 0.0016$ m. The distance between the leading edge of the airfoil and the trailing edge of the rod is equal to the airfoil chord $c = 0.1$ m, whereas the center of the rod is placed $1.5\,c$ downstream of a rectangular open-jet nozzle. The span is $3\,c$ for both rod and airfoil, which are placed between side plates. Kato's correction for acoustic computations [38], necessary for simulations with narrow spans, is hence not required in this case.

An isometric view of the setup is reported in Fig. 1 while a sketch with a side view of the simulation domain is shown in Fig. 2. The domain is a cube with sides equal to $40\,c$ centered at the leading-edge midspan, which is also the origin of the reference system with axes x in the streamwise direction, y in the vertical direction, and z in the spanwise direction.

The free-stream velocity of $72\,\mathrm{m\,s^{-1}}$ is obtained by prescribing the mass flow at the nozzle inlet. Zero-velocity inlet condition is imposed on the domain boundaries with the exception of the downstream face, where the outlet is assigned
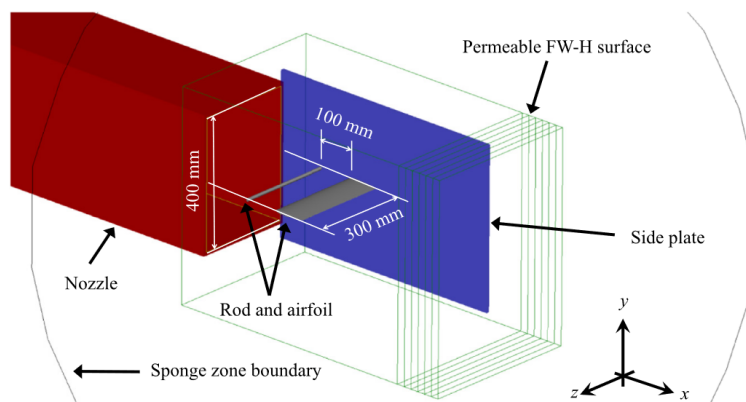
Fig. 1 Isometric view of the rod-airfoil setup. Image from Teruna *et al.* [23]
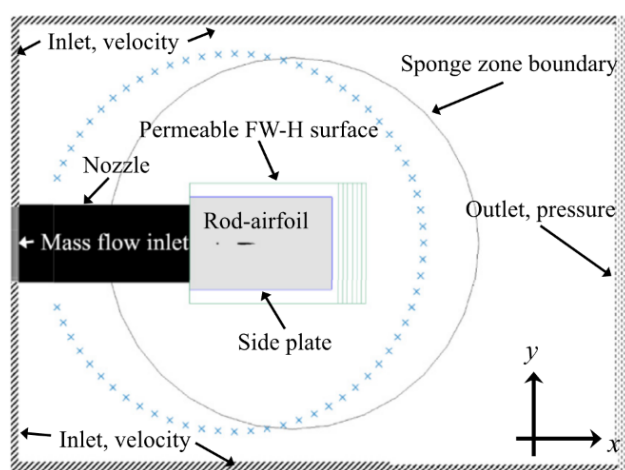

Fig. 2 Side view of the rod-airfoil setup (the outer boundaries are not drawn to scale). Microphone locations for far-field noise computation are indicated with blue crosses. Image from Teruna *et al.* [23]

with a static pressure of 100 kPa. In addition, all the solid surfaces, except for the nozzle walls, are defined as no-slip walls. To prevent the sound waves from being reflected by the boundaries, an acoustic buffer zone is defined outside of a spherical boundary enclosing the near-field region.

13 voxel refinement regions are defined in the simulation domain, with the finest grid dimension being $8 \times 10^{-3} d_{\text{rod}}$ near the rod. This implies that 125 voxels are assigned along the rod diameter, and the resulting average y^+ is 25 on the rod and 15 on the airfoil. In total, the simulation domain is discretized in 200×10^6 voxels in the finer configuration.

Both permeable and solid formulations of the FW-H analogy are used to compute the far-field noise. The results of the solid formulation considering only the airfoil surface are used as a reference to compare the implementation of Amiet's model. The acoustic pressure is acquired on the permeable FW-H surface with a sampling frequency of 29.5 Hz, while the surface pressure and quantities in the flow field have been recorded at a rate of 15 kHz. Welch's method with a Hanning window with 50 % overlap has been used to obtain the power spectral densities with a frequency resolution of 100 Hz. A physical timestep of 1.33×10^{-7} s for 67 flow passes along the airfoil chord has been used to carry out the simulation, resulting in a total physical time of 0.108 s if the transient of 10 flow passes is excluded. The simulation time is also equal to 150 vortex-shedding cycles.

To isolate the physics of the different turbulence scales, the band-pass filtering implemented in PowerACOUSTICS has been applied to the flow field. The filter is an optimized fast Fourier transform (FFT) with a trapezoidal window that tapers the first and last 5 % of the signal to zero without altering the central 90 %. The overall frequency band goes from 360 Hz to 7200 Hz, corresponding respectively to $St_{\text{d}} = 0.05$ and $St_{\text{d}} = 1$, where St_{d} is the Strouhal number calculated with respect to the rod diameter d_{rod}. This range, coincident with that considered by Teruna *et al.* [23], has been identified considering the sampling frequency used in the simulation and with the aim of discarding low-frequency

4

Table 1   Band-pass filter frequency bands. The Strouhal St_d is calculated with respect to the rod diameter and using the free-stream velocity U_∞.

Band	f_1	f_2	St_1	St_2
	Hz	Hz		
1	360	1800	0.05	0.25
2	1800	3600	0.25	0.50
3	3600	7200	0.50	1.00

inaccuracies in the spectral analysis. Three frequency bands have been identified to perform the band-pass filter (see Table 1). These bands have been selected to consider separately large-, mid-, and small-scale turbulence, with the vortex-shedding peak included in the low-frequency range. At the moment, these ranges have been set arbitrarily based on the analysis of the acoustic results obtained in the present work.

The directivity patterns have been calculated considering an arc in the $x - y$ plane with a radius of $R = 9.25\,c$ centered at the airfoil leading edge, with the points separated with a $10°$ increment and ranging from 0 to $\pm150°$. The upstream direction is at the angular position $\theta = 180°$, and the downstream one coincides with the angular position $\theta = 0°$. The results have been analyzed separately using three different Strouhal bands coincident with the bands used to perform the band-pass filter.

C. Amiet's model

A brief summary of Amiet's theory is provided hereafter. The notation used is consistent with that used by Amiet [39], but the axes (and consequently the notation for the velocity components) have been changed to be consistent with the reference system used in the present simulation: x is the streamwise (or horizontal) direction, whose velocity component is u, y is the upwash (or vertical) direction with v as velocity component and z is the crosswise (or lateral) direction with velocity component w. The model relies upon two simplifying hypotheses: the turbulence is supposed to be "frozen" in the convection and during the interaction, and the blade is considered to be an infinitely thin flat plate of chord $2b$ and with a large span $2d$ (therefore neglecting the effects of thickness, camber, and angle of attack). These hypotheses allow the incident gust with which the flat plate is interacting to be modeled as a two-dimensional upwash velocity gust with amplitude v_0 and transverse wavenumbers k_x and k_z, whose expression is

$$v_g = v_0 e^{i[k_x(U_\infty t - x) - k_z z]}, \tag{1}$$

U_∞ being the freestream velocity. The pressure jump across the flat plate is hence expressed as a function of this gust. By calculating the cross-spectral density of the surface pressure on the airfoil and using Curle's theory [40], the loading acting on the airfoil can be related to the far-field acoustic pressure S_{pp}, which is finally expressed as

$$S_{pp}(\boldsymbol{x}, \omega) = \left(\frac{\omega y \rho_\infty b}{c_\infty \sigma^2}\right)^2 \pi U_\infty d \int_{-\infty}^{+\infty} \frac{\sin^2\left[d\left(k_z + \frac{\omega z}{c_\infty \sigma}\right)\right]}{\left(k_z + \frac{\omega z}{c_\infty \sigma}\right)^2 \pi d} |\mathcal{L}(\boldsymbol{x}, K_x, k_z)|^2 \Phi_{vv}(K_x, k_z) \, dk_z, \tag{2}$$

where $\sigma = \sqrt{(x - x_0)^2 + \beta^2 \left[(y - y_0)^2 + (z - z_0)^2\right]}$ accounts for the effects of convection, with $\beta = \sqrt{1 - M^2}$ being the compressibility factor, and $\Phi_{vv}(K_x, k_z)$, with $K_x = \frac{-\omega}{U_\infty}$, is the two-dimensional wavenumber turbulence spectrum. The observer location is indicated with $\boldsymbol{x} = (x, y, z)$. $\mathcal{L}$ is the total aeroacoustic transfer function: it is derived as the sum of the leading-edge term $\mathcal{L}_1$ and trailing-edge term $\mathcal{L}_2$, which express the noise emitted by the primary scattering of the incoming turbulence at the leading edge and the back-scattering correction [41] of that incident field at the trailing edge, respectively. In the case of a flat plate, this function can be calculated analytically, while, for thicker airfoils, *ad hoc* numerical analyses must be carried out [42].

A simplified formulation of Amiet's model has been implemented in the present work. Equation 2 can indeed be simplified by assuming a large span and considering a listener in the midspan plane of the airfoil:

$$S_{pp}(x, y, 0, \omega) = \left(\frac{\omega y \rho_\infty b}{c_\infty \sigma_0^2}\right)^2 \pi U_\infty d \, |\mathcal{L}(\boldsymbol{x}, K_x, 0)|^2 \, \phi_{vv}(\omega) \, l_z(\omega), \tag{3}$$

5

where ϕ_{vv} is the power spectral density (PSD) of the vertical velocity fluctuations, and l_z is the spanwise coherence length of the velocity fluctuations impinging on the airfoil, calculated considering the spanwise distribution of the vertical velocity component in the same positions where the frequency spectrum has been sampled.

The aeroacoustic transfer function $\mathcal{L}$ has been implemented following the expression of de Santana *et al.* [11, 43] and reported hereafter:

$$\mathcal{L}_1 \left(x, y, z, k_x, k_y\right) = \frac{1}{\pi} \sqrt{\frac{2}{\left(\bar{k}_x + \beta^2\kappa\right)\theta_1}} \mathrm{E}^* \left(2\theta_1\right) \mathrm{e}^{\mathrm{i}\theta_2}; \tag{4}$$

$$\mathcal{L}_2 \left(x, y, z, k_x, k_y\right) \simeq \frac{\mathrm{e}^{\mathrm{i}\theta_2}}{\pi\theta_1\sqrt{2\pi\left(\bar{k}_x + \beta^2\kappa\right)}} \left\{ \mathrm{i}\left(1 - \mathrm{e}^{-2\mathrm{i}\theta_1}\right) + (1 - \mathrm{i})\left[\mathrm{E}^*\left(4\kappa\right) - \sqrt{\frac{2\kappa}{\theta_3}}\mathrm{e}^{-2\mathrm{i}\theta_1}\mathrm{E}^*\left(2\theta_3\right)\right] \right\}, \tag{5}$$

where $\theta_1 = \kappa - \mu x/\sigma_0$, $\theta_2 = \mu\left(M - x/\sigma_0\right) - \pi/4$, $\theta_3 = \kappa + \mu x/\sigma_0$, $\kappa^2 = \mu^2 - \bar{k}_z/\beta^2$, and $\mu = \bar{k}_x M/\beta^2$. The normalization of the wavenumbers is obtained by multiplying them by half the chord $c/2$, and is indicated by the symbol $(\bar{\cdot})$. The function $\mathrm{E}^*\left(x\right)$ is a combination of the Fresnel's integrals C_2 and S_2 with the following expression

$$\mathrm{E}^*\left(x\right) = \int_0^x \frac{\mathrm{e}^{-\mathrm{i}t}}{\sqrt{2\pi t}}\mathrm{d}t = C_2\left(x\right) - \mathrm{i}S_2\left(x\right);$$

with

$$C_2\left(x\right) = \frac{1}{\sqrt{2\pi}}\int_0^x \frac{\cos\left(t\right)}{\sqrt{t}}\mathrm{d}t;$$

$$S_2\left(x\right) = \frac{1}{\sqrt{2\pi}}\int_0^x \frac{\sin\left(t\right)}{\sqrt{t}}\mathrm{d}t.$$

These integrals have been calculated using a standard Matlab routine. Finally, the total aeroacoustic transfer function $\mathcal{L}$ is retrieved as the summation of the two contributions $\mathcal{L}_1$ and $\mathcal{L}_2$ above introduced. This formulation has been implemented using the commercial software Matlab.

D. Flow characterization

The integral length scale is computed to assess the scale of the turbulence structures the airfoil will interact with. It has been calculated using the formula from Pope [44], reported hereafter:

$$L_{ij}^m\left(\boldsymbol{x}, l\right) = \int_0^\infty R_{ij}^m\left(\boldsymbol{m}\right)\mathrm{d}l = \int_0^\infty \frac{\langle u_i\left(\boldsymbol{x} + l\boldsymbol{e}_m\right)u_j\left(\boldsymbol{x}\right)\rangle}{u_i\left(\boldsymbol{x}\right)u_j\left(\boldsymbol{x}\right)}\mathrm{d}l \quad . \tag{6}$$

$R_{ij}^m\left(x\right)$ is the correlation coefficient calculated with respect to a reference location x, u_i and u_j are the turbulent velocity fluctuations components in the ith and jth directions respectively, $\boldsymbol{e}_m$ is the unitary vector in the mth direction, and $l = \boldsymbol{l} \cdot \boldsymbol{e}_m$ is the separation length from the reference location. $\langle\cdot\rangle$ is the temporal-averaging operator with the assumption that the turbulent fluctuations in the rod wake are ergodic.

The results of the calculation are reported in Table 2. The expression is applied in Matlab using a discrete integration characterized by a spatial separation of $0.1\,d_{\mathrm{rod}}$ along the streamwise (or horizontal) direction x, the upwash (or vertical) direction y, and the crosswise (or lateral) direction z, whose respective velocity components are u, v, and w [23]. In the table, the ratios with respect to both rod diameter and leading-edge radius are shown. The latter, in particular, can be used as a criterion to understand the turbulence distortion mechanisms using the results of the RDT [45]. In this case, since the ratio between the integral length scales in the streamwise direction and the radius of the leading-edge circle is much larger than 1, we can conclude that the general behavior of turbulence in the interaction with the airfoil will follow the asymptotic case $\frac{L}{a} \gg 1$ of the RDT. This result implies that the present configuration can be rightfully used as a simplified model to assess the impact of turbulence distortion on the noise generation for wind turbine applications, for which the involved turbulence scales are much larger than the radius of the leading-edge circle.

III. Results

A. Turbulence-distortion mechanisms

The root-mean-square of the band-pass filtered velocity fluctuations along the stagnation streamline are shown in Fig. 3. It can be noticed that, in the vicinity of the airfoil, the trends of both horizontal and vertical velocity components

6

Table 2   Integral length scale L_{ij}^m in the rod wake at $2.5\,d_{\mathbf{rod}}$ upstream of the airfoil leading edge.

Ratio	L_{uu}^x	L_{vv}^y	L_{ww}^z
$\dfrac{L_{ij}^m}{d_{\text{rod}}}$	1.5	1.10	0.73
$\dfrac{L_{ij}^m}{r_{\text{LE}}}$	9.45	6.93	4.60

(a) Horizontal velocity component.

(b) Vertical velocity component.
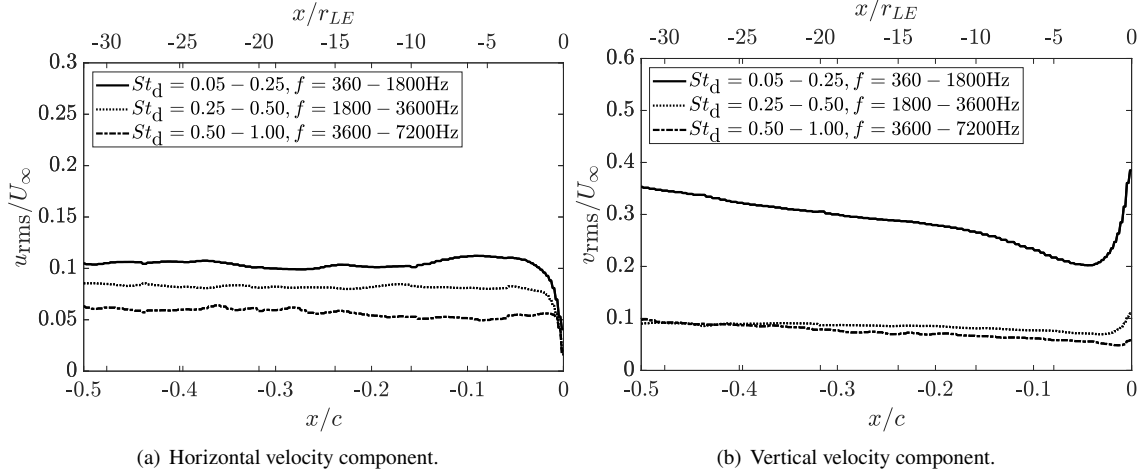
Fig. 3   Root-mean-square of the horizontal (left side) and vertical velocity (right side) component fluctuations along the stagnation streamline for different frequency bands (see Table 1).

abruptly change, as expected for the $\frac{L}{a} \gg 1$ asymptotic case according to the RDT. The horizontal component decreases near the stagnation point because of the blockage caused by the body, while the vertical one strongly increases because of the momentum transfer. These trends agree with the experimental and numerical results of Bearman [21] and Zamponi *et al.* [46]. Interestingly, the velocity fluctuations in the mid- and the high-frequency range (dotted and dash-dotted lines, respectively) change their trends at a distance that decreases with the increasing frequency.

In this regard, it is worth analyzing the velocity components turbulence spectra sampled along the stagnation streamline. Four positions have been identified by observing the trends of the root-mean-square of the velocity components with the purpose of accounting for the regions where the different turbulence scales start to be affected by the presence of the body. The distances of these sampling points with respect to the leading edge of the airfoil have been expressed as fractions of the airfoil chord and the radius of the leading edge (Table 3).

The frequency spectra of the horizontal and the vertical velocity components are reported in Fig. 4. The alteration of the velocity components due to turbulence distortion can be clearly recognized: the low- and the mid-frequency parts of the spectra, up to $St_{\text{d}} = 0.5$, corresponding to larger turbulence scales, decrease in the case of the horizontal component, whereas increase for the vertical velocity component, consistently with the analytical findings of the RDT and Zamponi [45] and the experimental measurements of Bearman [21]. The high-frequency part of the spectrum, on the other hand, despite the sampling performed very close to the stagnation point, is practically coincident for all the spectra for both the velocity components. This is a confirmation of the fact that the turbulence scales considered in the present configuration are much larger than the radius of the leading-edge circle, allowing hence to observe the physical mechanism characterizing the distortion of large turbulence scales.

This analysis shows that turbulence structures start to be affected by the presence of the airfoil at a distance that is proportional to their size: larger structures will start deforming more upstream than smaller ones. If this result, on the one hand, seems reasonable, on the other hand, it adds a new perspective to the conclusions of Mish and Devenport [47, 48] and de Santana *et al.* [11], who found that the effects of turbulence distortion can be recognized within $1r_{\text{LE}}$ from the stagnation point on the airfoil, therefore suggesting a dependence on the geometry of the body. The present result would indicate that the extension of the region where turbulence distortion occurs is related to the size of the turbulence structures involved. This finding mainly implies that an analysis of the inherent characteristics of the turbulence in the vicinity of the body must be carried out in order to thoroughly include the effects of turbulence distortion in the

7

Table 3   Upstream points coordinates along the stagnation streamline

Upstream Point	$\frac{x}{r_{LE}}$	$\frac{x}{c}$	Distance [m]
1	−0.31	−0.005	−0.0005
2	−0.63	−0.010	−0.001
3	−1.25	−0.020	−0.002
4	−6.25	−0.100	−0.010

(a) Horizontal velocity component frequency spectra.

(b) Vertical velocity component frequency spectra.
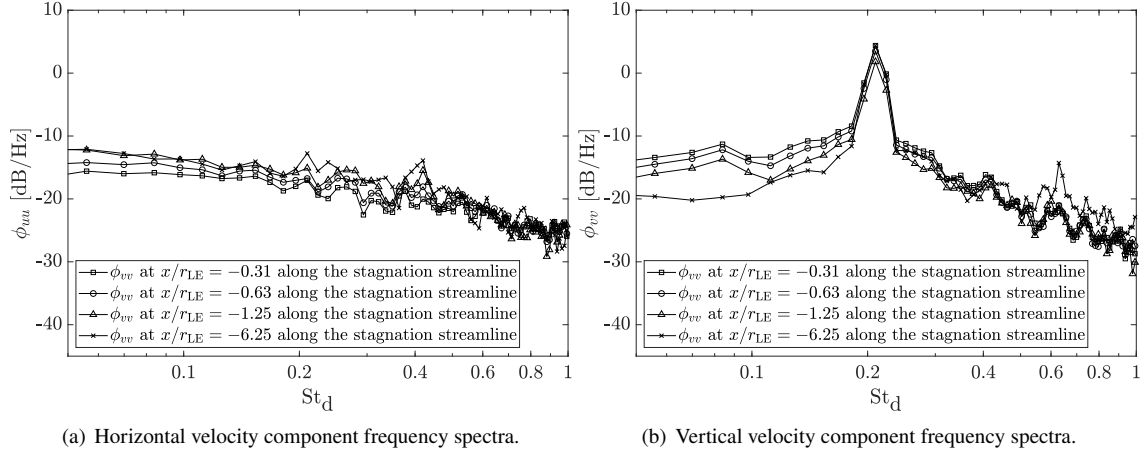
Fig. 4   Turbulence frequency spectra of the horizontal (left side) and vertical (right side) velocity components. The spectra have been sampled along the stagnation streamline at different distances from the airfoil leading edge.

modeling of the leading-edge noise generation mechanisms.

B. Impact of turbulence distortion on the surface pressure

The analysis of the surface pressure can provide information about the relation between the distortion mechanisms and noise generation, considering that, according to Curle's analogy [40], the unsteady loading distribution on the surface of the body is related to the far-field sound. Unsteady pressures along the airfoil surface have been considered in the midspan plane, similar to the velocity field in the previous subsection. The root-mean-square values of the surface pressure fluctuations are reported in Fig. 5 with respect to the curvilinear abscissa s. It is interesting to notice that the position along the airfoil surface where the pressure fluctuation is maximum is slightly downstream of the stagnation point. This result is consistent with the findings of Zamponi *et al.* [49], who considered a NACA-0024 interacting with the wake of an upstream circular rod. By comparing the trend of the root-mean-square of the surface pressure fluctuations with the time-averaged nondimensional pressure gradient along the airfoil in the streamwise direction, it can be shown that the position of maximum surface pressure fluctuations coincides with the pressure-gradient peak.

This physical observation identifies a connection between the pressure fluctuations on the surface, related to the noise generation, and the pressure gradient on the leading edge, which is instead linked to the pressure distribution along the airfoil and hence to the mean flow behavior around the body.

C. Application of Amiet's model

The results obtained by the analysis of the velocity field and the surface pressure are therefore used to keep into account the effects of turbulence distortion in Amiet's model. The proposed approach is to sample the vertical-velocity spectrum at the location of maximum surface-pressure fluctuations. The normal to the airfoil surface is considered at the peak location of the root-mean-square value of the surface-pressure fluctuations, and the spectrum is sampled at a
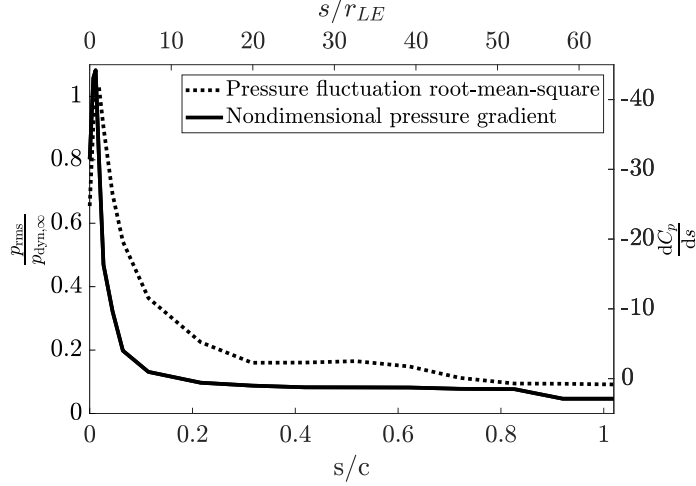
Fig. 5 Analysis of the surface pressure. The time-averaged pressure gradient in the midspan plane is compared with the root-mean-square of the surface pressure fluctuations.

distance of $0.3\,r_{\mathrm{LE}}$ from the airfoil surface to avoid sampling in the voxel closest to the surface of the body.

Amiet's model has been hence applied using Eq. 3. The observer location has been considered to be right above the leading edge ($\theta = 90\,\mathrm{deg}$) in the midspan plan at a distance of $R = 9.25c$. The solid formulation of the FW-H analogy has been used to calculate the noise prediction in the same observer position while neglecting the contribution coming from the rod. The result of the permeable formulation has been however reported for the sake of completeness.

The comparison between the analytical prediction and the FW-H analogy is reported in Fig. 6. A generally good agreement can be observed between the two methods for most parts of the frequency spectrum, although a significant discrepancy between the solid FW-H and Amiet's model is present for $St_{\mathrm{d}} > 0.7$ in terms of both slope of the spectrum and noise levels. However, it must also be noted that the abrupt fall of the solid FW-H at $St_{\mathrm{d}} > 0.7$ is due to the low sampling frequency imposed to acquire the surface pressure along the airfoil in the numerical simulation (area highlighted in grey in Fig. 6). Indeed, the results provided by the permeable formulation, for which the pressures have been acquired at twice the sampling frequency used on the airfoil surface, are not affected by this decay and feature a good match with the analytical prediction also in this frequency range.

The best agreement is found in the frequency range up to $St_{\mathrm{d}} \simeq 0.25$. For $0.25 < St_{\mathrm{d}} < 0.5$, the slope is correctly predicted, but a clear underestimation of the noise levels is present. Nevertheless, in the high-frequency part of the spectrum, the "distorted" spectrum provides again a satisfying match with the solid FW-H results up to the threshold of $St_{\mathrm{d}} = 0.7$

The conclusions drawn above are also confirmed by the far-field noise directivity patterns shown in Fig. 7. The results of the analytical prediction agree with those of the solid FW-H for all three Strouhal bands. The pattern predicted by Amiet's model overlaps with the one provided by the solid formulation of FW-H for the $0.05 < St_{\mathrm{d}} < 0.25$ band at all the angular positions. In the mid- and high-frequency range, it can be noticed that the directivity pattern is losing the dipolar shape observed for the low-frequency band plots, turning almost into a cardioid shape because of the noncoherent sound emission occurring in these frequency ranges from the leading edge. For the $0.25 < St\mathrm{d} < 0.5$ band, the shape of the directivity pattern is correctly predicted by Amiet's model, but it is also clear that an overall underestimation up to $5\,\mathrm{dB}$ is obtained at all angular positions with respect to the prediction provided by the FW-H analogy. In the high-frequency band ($0.5 < St_{\mathrm{d}} < 1$), a good agreement is again found. Indeed, Amiet's model correctly calculates the directivity pattern, with the exception of an overestimation of around $5\,\mathrm{dB}$ for the two lobes at $\theta = 30°$ and $\theta = 330°$.

IV. Conclusions

A novel approach to account for the effects of turbulence distortion in the prediction of leading-edge noise has been proposed in the present work. The analytical model developed by Amiet has been modified by considering in input a turbulence spectrum sampled in the flow-field region where the distortion occurs, to consider the alterations experienced by the velocity components near the airfoil leading edge and, consequently, their impact on the far-field noise.
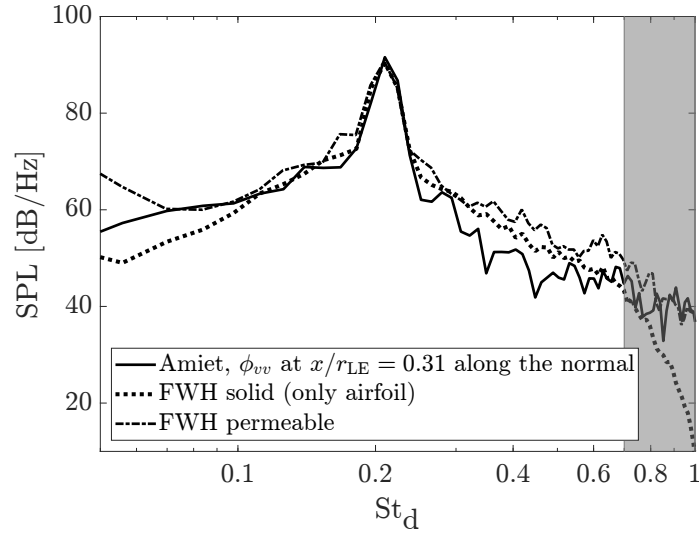
9

Fig. 6 Sound spectrum in the far-field calculated for an observer placed at $R = 9.25\,c$ and $\theta = 90°$, with the angular position computed with respect to the downstream direction. The results of Amiet's implementation considering the "distorted" spectrum as input are compared to the calculation provided by the solid formulation of the FW-H analogy. The reference pressure used to calculate the SPL is 2×10^{-5} Pa.

A rod-airfoil configuration has been selected to carry out the analysis of the vortex dynamics and generalize the acoustic investigation considering both broadband and tonal sound components. The trend of the root-mean-square values of the velocity fluctuations along the stagnation streamline in the vicinity of the airfoil leading edge are in agreement with the RDT predictions: the vertical-velocity component increases substantially at the expense of the horizontal one, which must decrease because of the no-penetration condition. The analysis of the band-pass filtered velocity fluctuations has shown that these distortion mechanisms start occurring at a distance from the stagnation point related to the size of the turbulent structures. This result suggests that turbulence distortion is not occurring within a distance from the body related to a geometrical characteristic but depends on the inherent dimensions of the scales involved in the interaction.

The surface pressure in the midspan plane has also been considered to investigate the effects of turbulence distortion on noise generation. From the analysis of the root-mean-square values, it arose that the highest surface-pressure fluctuations are obtained downstream of the stagnation point, at the position where the pressure gradient along the airfoil is peaking. This observation suggests that the noise-generation efficiency is related to the intensity of the pressure gradient and, hence, the flow acceleration around the leading edge.

The results of this study have been therefore used to modify Amiet's model by sampling the turbulence spectrum at the position where the pressure fluctuations are the largest: this analytical method has shown good agreement with the numerical results obtained with the FW-H analogy, in terms of both sound pressure levels and directivity patterns.

This study represents a first step toward a more thorough understanding of the relationship between turbulence distortion and leading-edge noise generation with the purpose of enhancing noise prediction by means of low-fidelity methods. Yet further investigations are necessary to investigate the behavior of the different turbulent structures in the interaction with the airfoil and to define and corroborate the impact of this physical mechanism on the surface pressure distribution.

Acknowledgments

$St_d = [0.05\text{-}0.25]$

(a) Low-frequency range.

$St_d = [0.25\text{-}0.5]$

(b) Mid-frequency range.

$St_d = [0.5\text{-}1]$
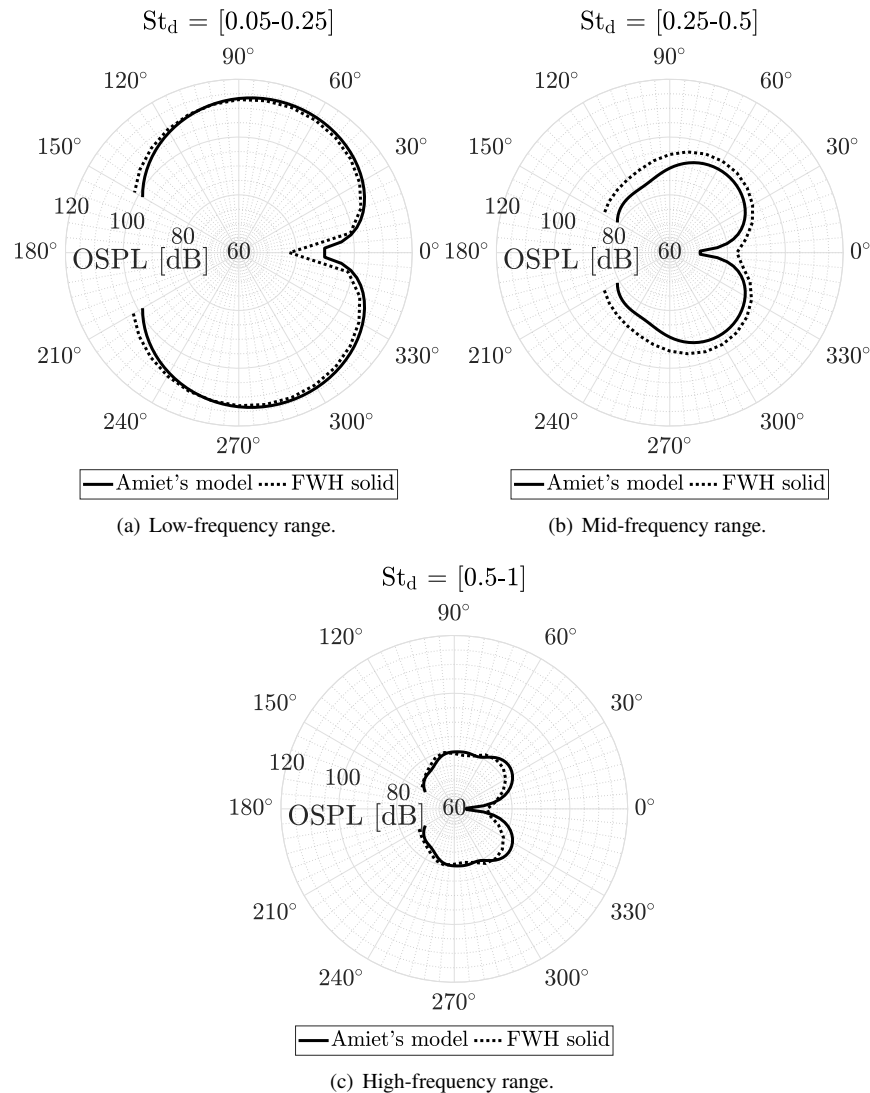

(c) High-frequency range.

Fig. 7   Far-field noise directivity patterns. Comparison of Amiet's Model with the "distorted" spectrum as input and the FW-H solid results.

References

[1] Grosveld, F. W., "Prediction of Broadband Noise from Horizontal Axis Wind Turbines," *Journal of Propulsion and Power*, Vol. 1, No. 4, 1985, pp. 292–299. https://doi.org/10.2514/3.22796.

[2] Moriarty, P., and Migliore, P., "Semi-Empirical Aeroacoustic Noise Prediction Code for Wind Turbines," Tech. Rep. NREL/TP-500-34478, 15006098, Dec. 2003. https://doi.org/10.2172/15006098.

[3] Oerlemans, S., Fisher, M., Maeder, T., and Kögler, K., "Reduction of Wind Turbine Noise Using Optimized Airfoils and Trailing-Edge Serrations," *AIAA Journal*, Vol. 47, No. 6, 2009, pp. 1470–1481. https://doi.org/10.2514/1.38888.

[4] Ricciardelli, F., and Polimeno, S., "Some Characteristics of the Wind Flow in the Lower Urban Boundary Layer," *Journal of Wind Engineering and Industrial Aerodynamics*, Vol. 94, No. 11, 2006, pp. 815–832. https://doi.org/10.1016/j.jweia.2006.06.003.

[5] Fernando, H., "Fluid Dynamics of Urban Atmospheres in Complex Terrain," *Annual Review of Fluid Mechanics*, Vol. 42, 2009, pp. 365–389. https://doi.org/10.1146/annurev-fluid-121108-145459.

[6] Botero Bolivar, L., dos Santos, F. L., Venner, C., and Santana, L., *The Increase of the Airfoil Trailing Edge Noise and Unsteady Surface Pressure Due to High Inflow Turbulence*, 2021.

11

[7] Amiet, R. K., "Acoustic Radiation from an Airfoil in a Turbulent Stream," *Journal of Sound and Vibration*, Vol. 41, No. 4, 1975, pp. 407–420. https://doi.org/10.1016/S0022-460X(75)80105-2.

[8] Lowson, M., "Theory and Experiment for Wind Turbine Noise," *32nd Aerospace Sciences Meeting and Exhibit*, American Institute of Aeronautics and Astronautics, Reno,NV,U.S.A., 1994. https://doi.org/10.2514/6.1994-119.

[9] Guidati, G., Bareiss, R., Wagner, S., Parchen, R., Guidati, G., Bareiss, R., Wagner, S., and Parchen, R., "Simulation and Measurement of Inflow-Turbulence Noise on Airfoils," *3rd AIAA/CEAS Aeroacoustics Conference*, American Institute of Aeronautics and Astronautics, Atlanta,GA,U.S.A., 1997. https://doi.org/10.2514/6.1997-1698.

[10] Moreau, S., and Roger, M., "Effect of Angle of Attack and Airfoil Shape on Turbulence-Interaction Noise," *11th AIAA/CEAS Aeroacoustics Conference*, American Institute of Aeronautics and Astronautics, Monterey, California, 2005. https://doi.org/10.2514/6.2005-2973.

[11] De Santana, L. D., Christophe, J., Schram, C., and Desmet, W., "A Rapid Distortion Theory Modified Turbulence Spectra for Semi-Analytical Airfoil Noise Prediction," *Journal of Sound and Vibration*, Vol. 383, 2016, pp. 349–363. https://doi.org/10.1016/j.jsv.2016.07.026.

[12] dos Santos, F. L., Botero-Bolívar, L., Venner, C., and de Santana, L. D., "Modeling the Turbulence Spectrum Dissipation Range for Leading-Edge Noise Prediction," *AIAA Journal*, 2022, pp. 1–12. https://doi.org/10.2514/1.J061106.

[13] Moreau, S., and Roger, M., "Competing Broadband Noise Mechanisms in Low-Speed Axial Fans," *AIAA Journal*, Vol. 45, No. 1, 2007, pp. 48–57. https://doi.org/10.2514/1.14583.

[14] Paterson, R., and Amiet, R., "Acoustic Radiation and Surface Pressure Characteristics of an Airfoil Due to Incident Turbulence," *3rd Aeroacoustics Conference*, Aeroacoustics Conferences, American Institute of Aeronautics and Astronautics, 1976. https://doi.org/10.2514/6.1976-571.

[15] Paterson, R. W., and Amiet, R. K., "Noise of a Model Helicopter Rotor Due to Ingestion of Turbulence," Tech. Rep. NASA-CR-3213, Nov. 1979.

[16] Dassen, T., Parchen, R., and Bruggeman, J., "Wind Tunnel Measurements of the Aerodynamic Noise of Blade Sections," *European Wind Energy Conference and Exhibition*, Thessaloniki, 1993.

[17] Moriarty, P., Guidati, G., and Migliore, P., "Recent Improvement of a Semi-Empirical Aeroacoustic Prediction Code for Wind Turbines," *10th AIAA/CEAS Aeroacoustics Conference*, American Institute of Aeronautics and Astronautics, Manchester, GREAT BRITAIN, 2004. https://doi.org/10.2514/6.2004-3041.

[18] Buck, S., Oerlemans, S., and Palo, S., "Experimental Validation of a Wind Turbine Turbulent Inflow Noise Prediction Code," *AIAA Journal*, Vol. 56, No. 4, 2018, pp. 1495–1506. https://doi.org/10.2514/1.J056134.

[19] Christophe, J., "Application of Hybrid Methods to High Frequency Aeroacoustics," Ph.D. thesis, 2011.

[20] Hunt, J. C. R., "A Theory of Turbulent Flow Round Two-Dimensional Bluff Bodies," *J. Fluid Mech.*, Vol. 61, No. 4, 1973, pp. 625–706. https://doi.org/10.1017/S0022112073000893.

[21] Bearman, P. W., "Some Measurements of the Distortion of Turbulence Approaching a Two-Dimensional Bluff Body," *J. Fluid Mech.*, Vol. 53, No. 03, 1972, p. 451. https://doi.org/10.1017/S0022112072000254.

[22] Britter, R. E., Hunt, J. C. R., and Mumford, J. C., "The Distortion of Turbulence by a Circular Cylinder," *Journal of Fluid Mechanics*, Vol. 92, No. 2, 1979, pp. 269–301. https://doi.org/10.1017/S0022112079000628.

[23] Teruna, C., Avallone, F., Casalino, D., and Ragni, D., "Numerical Investigation of Leading Edge Noise Reduction on a Rod-Airfoil Configuration Using Porous Materials and Serrations," *Journal of Sound and Vibration*, Vol. 494, 2021, p. 115880. https://doi.org/10.1016/j.jsv.2020.115880.

[24] Jacob, M. C., Boudet, J., Casalino, D., and Michard, M., "A Rod-Airfoil Experiment as a Benchmark for Broadband Noise Modeling," *Theor. Comput. Fluid Dyn.*, Vol. 19, No. 3, 2005, pp. 171–196. https://doi.org/10.1007/s00162-004-0108-6.

[25] Casalino, D., Avallone, F., Gonzalez-Martino, I., and Ragni, D., "Aeroacoustic Study of a Wavy Stator Leading Edge in a Realistic Fan/OGV Stage," *Journal of Sound and Vibration*, Vol. 442, 2019, pp. 138–154. https://doi.org/10.1016/j.jsv.2018.10.057.

[26] Satti, R., Lew, P.-T., Li, Y., Shock, R., and Noelting, S., "Unsteady Flow Computations and Noise Predictions on Rod-Airfoil Using Lattice Boltzmann Method," *47th AIAA Aerospace Sciences Meeting Including The New Horizons Forum and Aerospace Exposition*, American Institute of Aeronautics and Astronautics, Orlando, Florida, 2009. https://doi.org/10.2514/6.2009-497.

[27] Teruna, C., Ragni, D., Avallone, F., and Casalino, D., "A Rod-Linear Cascade Model for Emulating Rotor-Stator Interaction Noise in Turbofans: A Numerical Study," *Aerospace Science and Technology*, Vol. 90, 2019. https://doi.org/10.1016/j.ast.2019.04.047.

[28] Chen, H., Chen, S., and Matthaeus, W. H., "Recovery of the Navier-Stokes Equations Using a Lattice-Gas Boltzmann Method," *Phys. Rev. A*, Vol. 45, No. 8, 1992, pp. R5339–R5342. https://doi.org/10.1103/PhysRevA.45.R5339.

[29] Bhatnagar, P. L., Gross, E. P., and Krook, M., "A Model for Collision Processes in Gases. I. Small Amplitude Processes in Charged and Neutral One-Component Systems," *Phys. Rev.*, Vol. 94, No. 3, 1954, pp. 511–525. https://doi.org/10.1103/PhysRev.94.511.

[30] Chen, H., Kandasamy, S., Orszag, S., Shock, R., Succi, S., and Yakhot, V., "Extended Boltzmann Kinetic Equation for Turbulent Flows," *Science*, Vol. 301, No. 5633, 2003, pp. 633–636. https://doi.org/10.1126/science.1085048.

[31] Yakhot, V., and Orszag, S. A., "Renormalization Group Analysis of Turbulence. I. Basic Theory," *J Sci Comput*, Vol. 1, No. 1, 1986, pp. 3–51. https://doi.org/10.1007/BF01061452.

[32] Chen, H., Orszag, S. A., Staroselsky, I., and Succi, S., "Expanded Analogy between Boltzmann Kinetic Theory of Fluids and Turbulence," *Journal of Fluid Mechanics*, Vol. 519, 2004, pp. 301–314. https://doi.org/10.1017/S0022112004001211.

[33] Chen, H., Teixeira, C., and Molvig, K., "Realization of Fluid Boundary Conditions via Discrete Boltzmann Dynamics," *Int. J. Mod. Phys. C*, Vol. 09, No. 08, 1998, pp. 1281–1292. https://doi.org/10.1142/S0129183198001151.

[34] Launder, B. E., and Spalding, D. B., "The Numerical Computation of Turbulent Flows," *Numerical Prediction of Flow, Heat Transfer, Turbulence and Combustion*, edited by S. V. Patankar, A. Pollard, A. K. Singhal, and S. P. Vanka, Pergamon, 1983, pp. 96–116. https://doi.org/10.1016/B978-0-08-030937-8.50016-7.

[35] Williams, J. E. F., and Hawkings, D. L. H. R., "Sound Generation by Turbulence and Surfaces in Arbitrary Motion," *Philosophical Transactions of the Royal Society of London. Series A, Mathematical and Physical Sciences*, Vol. 264, No. 1151, 1969, pp. 321–342.

[36] Farassat, F., and Succi, G. P., "A Review of Propeller Discrete Frequency Noise Prediction Technology with Emphasis on Two Current Methods for Time Domain Calculations," *Journal of Sound and Vibration*, Vol. 71, No. 3, 1980, pp. 399–419. https://doi.org/10.1016/0022-460X(80)90422-8.

[37] Casalino, D., "An Advanced Time Approach for Acoustic Analogy Predictions," *Journal of Sound and Vibration*, Vol. 261, No. 4, 2003, pp. 583–612. https://doi.org/10.1016/S0022-460X(02)00986-0.

[38] Kato, C., Iida, A., Takano, Y., Fujita, H., and Ikegawa, M., "Numerical Prediction of Aerodynamic Noise Radiated from Low Mach Number Turbulent Wake," *31st Aerospace Sciences Meeting*, American Institute of Aeronautics and Astronautics, Reno,NV,U.S.A., 1993. https://doi.org/10.2514/6.1993-145.

[39] Amiet, R. K., "Noise Due to Turbulent Flow Past a Trailing Edge," *Journal of Sound and Vibration*, Vol. 47, No. 3, 1976, pp. 387–393. https://doi.org/10.1016/0022-460X(76)90948-2.

[40] Curle, N., and Lighthill, M. J., "The Influence of Solid Boundaries upon Aerodynamic Sound," *Proceedings of the Royal Society of London. Series A. Mathematical and Physical Sciences*, Vol. 231, No. 1187, 1955, pp. 505–514. https://doi.org/10.1098/rspa.1955.0191.

[41] Roger, M., and Moreau, S., "Back-Scattering Correction and Further Extensions of Amiet's Trailing-Edge Noise Model. Part 1: Theory," *Journal of Sound and Vibration*, Vol. 286, No. 3, 2005, pp. 477–506. https://doi.org/10.1016/j.jsv.2004.10.054.

[42] Miotto, R. F., Wolf, W. R., and de Santana, L. D., "Leading-Edge Noise Prediction of General Airfoil Profiles with Spanwise-Varying Inflow Conditions," *AIAA Journal*, Vol. 56, No. 5, 2018, pp. 1711–1716. https://doi.org/10.2514/1.J056716.

[43] De Santana, L. D., "Semi-Analytical Methodologies for Airfoil Noise Prediction," Ph.D. thesis, 2015.

[44] Pope, S. B., "Turbulent Flows," , Aug. 2000.

[45] Zamponi, R., Moreau, S., and Schram, C., "Rapid Distortion Theory of Turbulent Flow around a Porous Cylinder," *J. Fluid Mech.*, Vol. 915, 2021, p. A27. https://doi.org/10.1017/jfm.2021.8.

[46] Zamponi, R., Satcunanathan, S., Moreau, S., Ragni, D., Meinke, M., Schröder, W., and Schram, C., "On the Role of Turbulence Distortion on Leading-Edge Noise Reduction by Means of Porosity," *Journal of Sound and Vibration*, Vol. 485, 2020, p. 115561. https://doi.org/10.1016/j.jsv.2020.115561.

[47] Mish, P. F., and Devenport, W. J., "An Experimental Investigation of Unsteady Surface Pressure on an Airfoil in Turbulence—Part 1: Effects of Mean Loading," *Journal of Sound and Vibration*, Vol. 296, No. 3, 2006, pp. 417–446. https://doi.org/10.1016/j.jsv.2005.08.008.

[48] Mish, P. F., and Devenport, W. J., "An Experimental Investigation of Unsteady Surface Pressure on an Airfoil in Turbulence—Part 2: Sources and Prediction of Mean Loading Effects," *Journal of Sound and Vibration*, Vol. 296, No. 3, 2006, pp. 447–460. https://doi.org/10.1016/j.jsv.2005.08.009.

[49] Zamponi, R., Satcunanathan, S., Moreau, S., Meinke, M., Schröder, W., and Schram, C., "Effect of Porosity on Curle's Dipolar Sources on an Aerofoil in Turbulent Flow," *Journal of Sound and Vibration*, Vol. 542, 2023, p. 117353. https://doi.org/10.1016/j.jsv.2022.117353.